MetaResource vol. XX, no. X, pp. 1–XX, 202X
DOI: 10.23919/METAR.2026.000048
Original Article

LSTM learning enhanced deep cone thickening and paste backfilling for high density tailings: A case study

Ruiming Guo[1,3,✉], Bolin Xiao[1,2,✉], Jun Nie[1,4], Aixiang Wu[2], Jiandong Wang[3], and Min Liu[4]

[1] *China-Zambia Belt and Road Joint Laboratory on Green and Safe Development of Mineral Resources, University of Science and Technology Beijing, Beijing 100083, China*

[2] *State Key Laboratory of High-Efficient Mining and Safety of Metal Mine Ministry of Education, University of Science and Technology Beijing, Beijing 100083, China*

[3] *Key Laboratory of Safe and Green Mining of Metal Mines with Cemented Paste Backfill of the National Mine Safety Administration, University of Science and Technology Beijing, Beijing 100083, China*

[4] *China Nonferrous Metal Mining Group Co., Ltd., Beijing 100029, China*

Received: 12 Dec 2025
Revised: 3 Feb 2026
Accepted: 4 Feb 2026
Online: xx xxx xxxx

KEYWORDS

paste backfill,
deep cone thickening,
high-density tailings,
long short-term memory (LSTM),
underflow concentration prediction

ABSTRACT

Paste backfill relying on deep-cone thickening represents a complex systems engineering challenge. Achieving stable thickening, consistent paste quality, and efficient process control remains a critical challenge for the metal mining industry. Recent advances in computational intelligence offer new opportunities to improve system efficiency and operational stability. Using data from a Mongolian zinc mine with high-specific-gravity tailings (SG = 3.459), this study proposes a multivariate long short-term memory (LSTM)-based predictive model for underflow concentration. Leveraging historical data on four key variables, the model employs a sliding-window mechanism to perform recursive three-hour-ahead forecasts of underflow concentration. The model achieved high training accuracy (coefficient of determination (R^2) = 0.92) and robust test performance (mean absolute error (MAE) = 0.42% and root mean squared error (RMSE) = 0.48%), confirming its suitability for engineering applications. Simulations under three discharge rates (40, 50, 60 m^3/h) indicated that solely maximizing discharge rate is suboptimal. Accordingly, a "predicting–evaluating–regulating" feedforward control framework is proposed, shifting operations from reactive feedback to proactive regulation. Industrial trials maintained a slurry bed height of approximately 5.5 m. Proactive discharge-rate regulation sustained underflow concentration at 70%–82% for 7 h, enabling consistent preparation of high-quality paste (74%–76% solids content). In the stope, the backfill provided sufficient bearing capacity for personnel access within 10 h

Address correspondence to Ruiming Guo: grm220523@163.com; Bolin Xiao: bxiao@ustb.edu.cn

© The author(s) 2026. The articles published in this open access journal are distributed under the terms of the Creative Commons Attribution 4.0 International License (http://creativecommons.org/licenses/by/4.0/).

有斜出版 YOUKE PUBLISHING EXCLUSIVELY AVAILABLE VIA IEEE Xplore DIGITAL LIBRARY

at low cement-to-tailings ratios, achieving 1.5 MPa after one day and exceeding 3 MPa after three days at higher ratios. The proposed predictive model offers a quantitative tool and a methodological pathway for optimizing discharge strategies and facilitating feedforward control in deep-cone thickening.

1 Introduction

Paste backfill technology, a pivotal method for safe and efficient underground metal mining, effectively controls rock mass movement in stopes, enhances resource recovery, and significantly reduces surface tailings discharge and the need for new tailings dams [1, 2]. Preparing paste backfill by mixing high-concentration tailings with binders at specific ratios represents a key technical pathway toward achieving green mining and minimizing tailings disposal [3]. The primary step in the paste filling process involves concentrating tailings through deep cone thickening to produce a high-solids, high-viscosity underflow [4]. Compared to conventional thickeners, deep cone thickeners feature deeper compression zones and greater slurry bed depths. They can achieve underflow solids concentrations of 70%–80% or higher within smaller footprints, providing the high-concentration feedstock required for paste filling while reducing the load on subsequent dewatering processes [1]. However, the rapid settling and intense compaction of high-density tailings within deep cone thickener (DCT) can lead to challenges, including rapid rises in slurry bed height and sustained pressure buildup. This necessitates a trade-off between the underflow properties (pumpability and stackability) and the equipment load [5].

In the deep-cone thickening of high-density tailings, the yield stress and viscosity of the slurry bed escalate, substantially raising the torque required for rake agitation and discharge. Improper control of feed conditions or discharge rates can cause sudden torque spikes, rake arm bogging, bed instability, or even catastrophic "rake jamming". Furthermore, short-term fluctuations in underflow concentration and flow rate directly affect paste preparation and pipeline transport. These fluctuations induce significant variations in paste rheology and transport resistance, increasing the risk of blockages and compromising filling quality [6]. Industrial practice indicates that relying solely on manual adjustments based on instantaneous torque, bed depth, and visual inspection often fails to detect accumulation trends over multi-hour timeframes. Consequently, optimizing underflow discharge strategies to simultaneously prevent thickener overload and pipeline blockages remains a systemic challenge.

Extensive research has addressed the mechanistic modeling, process optimization, and advanced control of deep-cone thickening for whole tailings [7, 8]. Traditional approaches primarily rely on theories of hindered settling and compressive consolidation. By coupling sedimentation kinetics, consolidation equations, and yield stress–volume fraction relationships, one-dimensional (1D) or multi-dimensional mechanistic models were developed to describe the steady-state and dynamic behavior of bed depth, underflow concentration, and rake torque. Consequently, dynamic models for industrial-scale thickeners evolved, facilitating advanced control strategies like model predictive control (MPC) to enhance underflow stability and overflow clarity [9–11]. Recent studies systematically analyzed operational fluctuations, revealing that underflow concentration, flow rate, and bed load exhibit significant variability under diverse operating conditions. This variability is a primary driver of instability in downstream conveying, pumping, and stacking performance [8, 10]. However, few case studies have addressed the applicability of these strategies to high-specific-gravity tailings, particularly iron-rich whole tailings.

Driven by rapid advancements in industrial process monitoring and computational power, data-driven soft measurement and prediction methods have emerged as a pivotal research direction for thickening processes. Long short-term memory (LSTM) networks and their variants have demonstrated superior performance in predicting key indicators of complex

industrial processes, owing to their proficiency in modeling nonlinear, multivariate, and long-term dependencies [12, 13]. However, existing research has primarily focused on short-term prediction under fixed operating conditions or single discharge scenarios [14], often overlooking the dynamic coupling among discharge rate, bed load, and the multi-hour evolution of underflow concentration in paste filling applications.

Focusing on the Ovoo Zinc Mine in Mongolia, this paper presents an engineering case study on the efficient thickening and paste filling of whole tailings with a high specific gravity of 3.459. First, the key parameters of Mongolia's inaugural paste filling system are detailed. Subsequently, utilizing industrial commissioning data, a multivariate LSTM-based model was developed to predict underflow concentration. The model incorporates feed concentration, feed rate, bed depth, discharge rate, and underflow concentration as input variables. This enables the prediction of thickener underflow concentration over a 3 h horizon under varying discharge conditions. This approach provides a quantitative basis for setting discharge rates and implementing feedforward control, offering a new technical pathway to mitigate rake torque risks and optimize the system-level operation of deep-cone thickeners processing high-specific-gravity tailings. The paper concludes by summarizing the primary achievements of this case study.

2 Engineering background

2.1 Tailings characteristics

The specific gravity of the whole tailings from the Zinc Ovoo Mine was determined to be 3.459 using the pycnometer method, characterizing them as high-specific-gravity tailings. The particle size distribution, determined via laser diffraction, is illustrated in Figure 1. Analysis reveals that 16.40%, 23.84%, and 32.85% of the particles are finer than 5, 10, and 20 μm, respectively, and 59.48% pass through a 200-mesh (75 μm) sieve. Overall, the particle size distribution is considered relatively coarse. The chemical composition, obtained via X-ray fluorescence (XRF) analysis, is presented in Table 1. Notably, the Fe_2O_3 content was measured at 32.9%. This high iron content is the primary factor contributing to the elevated specific gravity and may pose challenges to the flocculation and thickening processes.

2.2 Filling system overview

The paste filling system at the Ovoo Zinc Mine comprises several major subsystems: tailings feed, deep cone thickening, binder addition, paste mixing, pipeline transport, and automatic control. Tailings slurry with a mass concentration of 45%–50%, produced by the concentrator, is pumped via the pumping station to the DCT. The underflow concentration is thickened to 70%–82%, with a high-level circulation system installed to prevent rake jamming under excessive torque conditions. The underflow is then pumped into a two-stage mixer and blended with binders and dilution water to form a paste with a solids content of approximately 74%–76%. This paste is transported via gravity flow at a rate of approximately 50 m^3/h to the underground stopes. The process flowchart of the paste filling system is illustrated in Figure 2.

2.2.1 Hardware configuration

(1) Tailings feed pipeline

Two slurry pumps are employed to transport

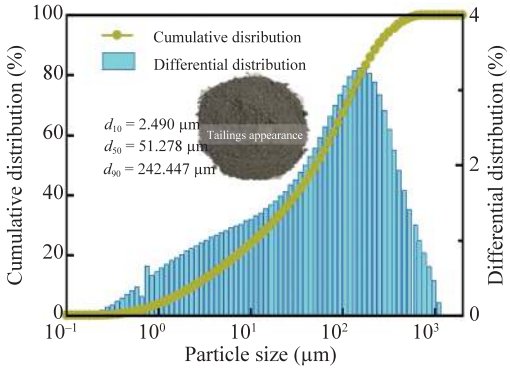

Figure 1 Particle size distribution curve of tailings

Table 1 Chemical composition of tailings

Component	Fe_2O_3	SiO_2	CaO	MnO	Al_2O_3	MgO	SO_3	ZnO	Na_2O	K_2O	Others
wt.%	32.894	26.251	21.475	11.876	3.133	1.654	0.875	0.616	0.436	0.268	0.522

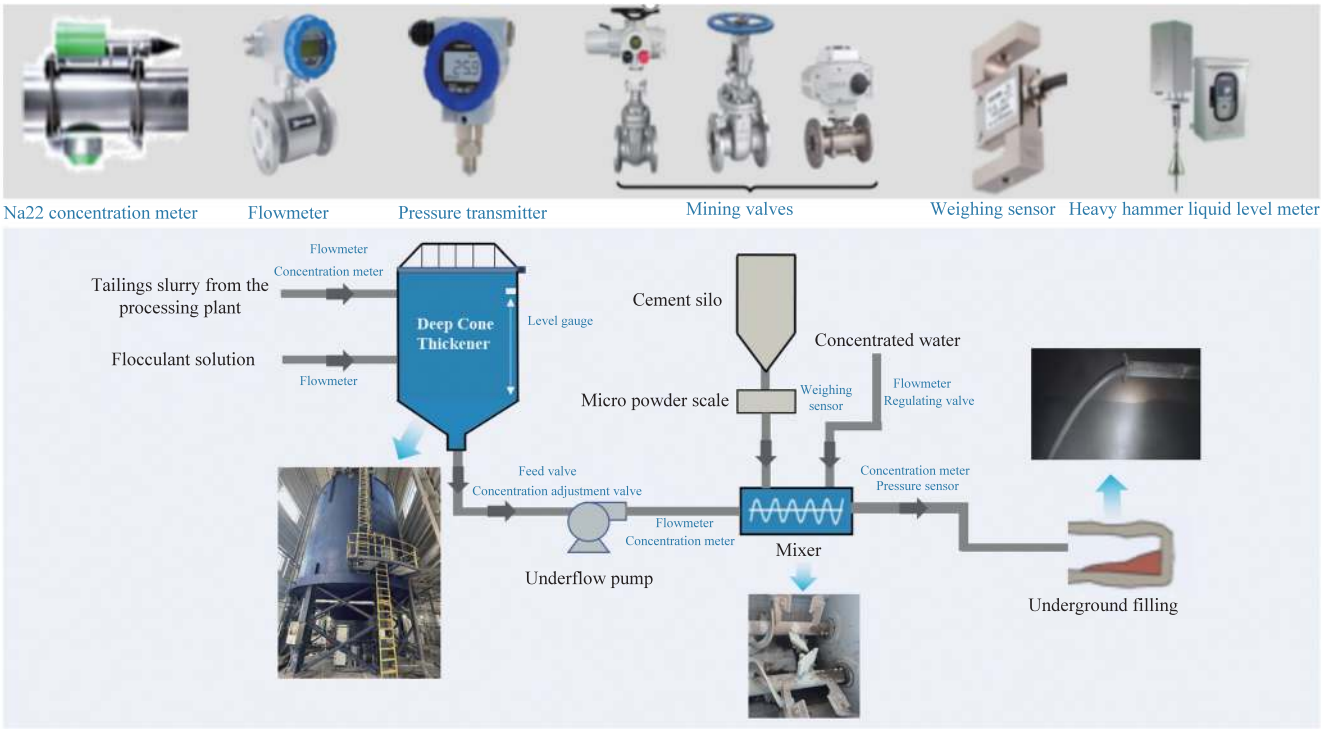

Figure 2 Process flowchart of the paste filling system

tailings from the concentrator to the backfill station. The feed pipeline spans 1,980 m with a maximum elevation gain of approximately 54 m. The slurry pumps (Model 50ZS-50) have a rated flow capacity of 70 m^3/h and a head of 90 m. The pipeline is constructed from 16Mn wear-resistant seamless steel pipes connected via quick couplings. Electric heat tracing and thermal insulation are installed to prevent slurry freezing and pipeline blockages in cold environments.

(2) Deep cone thickening system

The site employs an FLSmidth deep cone thickener featuring an 8 m diameter, a 9 m cylindrical section height, a 3.8 m cone height, and a 30° cone angle. The drive unit utilizes two MX1500A-2 motors, each rated at 5.5 kW. The equipment is integrated with a control system, a flocculant dosing system, a tailings inlet, and a submersible feed dilution pump. A rake assembly and underflow cone scraper are installed on the lower vertical shaft. Their rotation facilitates slurry bed agitation and mechanical discharge.

The flocculant used is SNF DRYFLOC-615V, prepared at a concentration of 0.1%–0.5%. It is conveyed by a screw pump to the top of the thickener, subjected to a tenfold dilution, and then injected into the feed well via two distribution lines.

(3) Binder dosing and paste preparation

Binders are pneumatically conveyed from bulk tankers to a 400 m^3 vertical silo. Binder is routed through a steady-flow feeder, a single-tube metering scale, and a screw feeder for precise dosing. It is then fed into a twin-shaft mixer at preset proportions. The scale has a capacity of 3–20 t/h and employs variable frequency control to ensure precise binder addition.

Paste preparation utilizes a two-stage horizontal twin-shaft mixing process. A pinch valve and level sensor are installed between the mixers to automate flow and level control. The binder-to-tailings ratio ranges0 from 1:4 to 1:20, with a system design capacity of 50–60 m^3/h.

(4) Pipeline transport and instrumentation

The mixed paste is conveyed via gravity flow through the borehole. A pinch valve beneath the secondary mixer regulates the flow rate into the feed hopper. A 3 mm screen within the hopper prevents oversize particles from blocking the borehole. A flushing line is installed alongside. Between the hopper and borehole, a straight pipe section is equipped with a non-contact radiometric density gauge (^{22}Na source) and an electromagnetic flowmeter. The borehole casing consists of bimetallic composite pipe (Φ152 mm × 20 mm).

2.2.2 Control software system

The filling system employs an automated control architecture anchored by a distributed control system. Through the coordinated operation of subsystems, it achieves comprehensive online monitoring and automatic regulation of paste consistency, mix ratios, flow rates, and tank levels. The human–machine interface is depicted in Figure 3. The system incorporates critical components including flowmeters, radiometric density gauges, bin level sensors, slurry bed level sensors, and pinch valves. It features equipment interlocking, fault alarming, trend logging, and production reporting. To mitigate rake torque risks during high-load thickening and enhance process stability, an LSTM-based predictive control strategy for underflow concentration was developed using data from system commissioning.

3 Methodology

3.1 Problem definition and data processing

Targeting the underflow concentration at the Ovoo Zinc Mine, a model was constructed to correlate the dynamic interplay among discharge rate, bed load, and the multi-hour evolution of underflow concentration. Collected process variables included timestamp, feed concentration (%), feed flow rate (m^3/h), bed depth (m), and discharge flow rate (m^3/h), with underflow concentration (%) serving as the target variable. To ensure high data fidelity, the underflow concentration measurements were calibrated using on-site rapid drying tests (gravimetric method). While this rigorous process constrained the sampling frequency, it ensured that the model was trained on reliable physical values. In instances where fewer than 50 valid records existed, the sequence was resampled at 5-min intervals, and missing points were imputed using time-based interpolation. Subsequently, the selected variables constituted the feature matrix. Both features and targets were normalized using Z-score standardization (Equation (1)) to eliminate scale discrepancies and enhance numerical stability during training.

$$Z_{ij} = \frac{x_{ij} - \mu_j}{\sigma_j} \tag{1}$$

where x_{ij} denotes the j-th feature value of the i-th

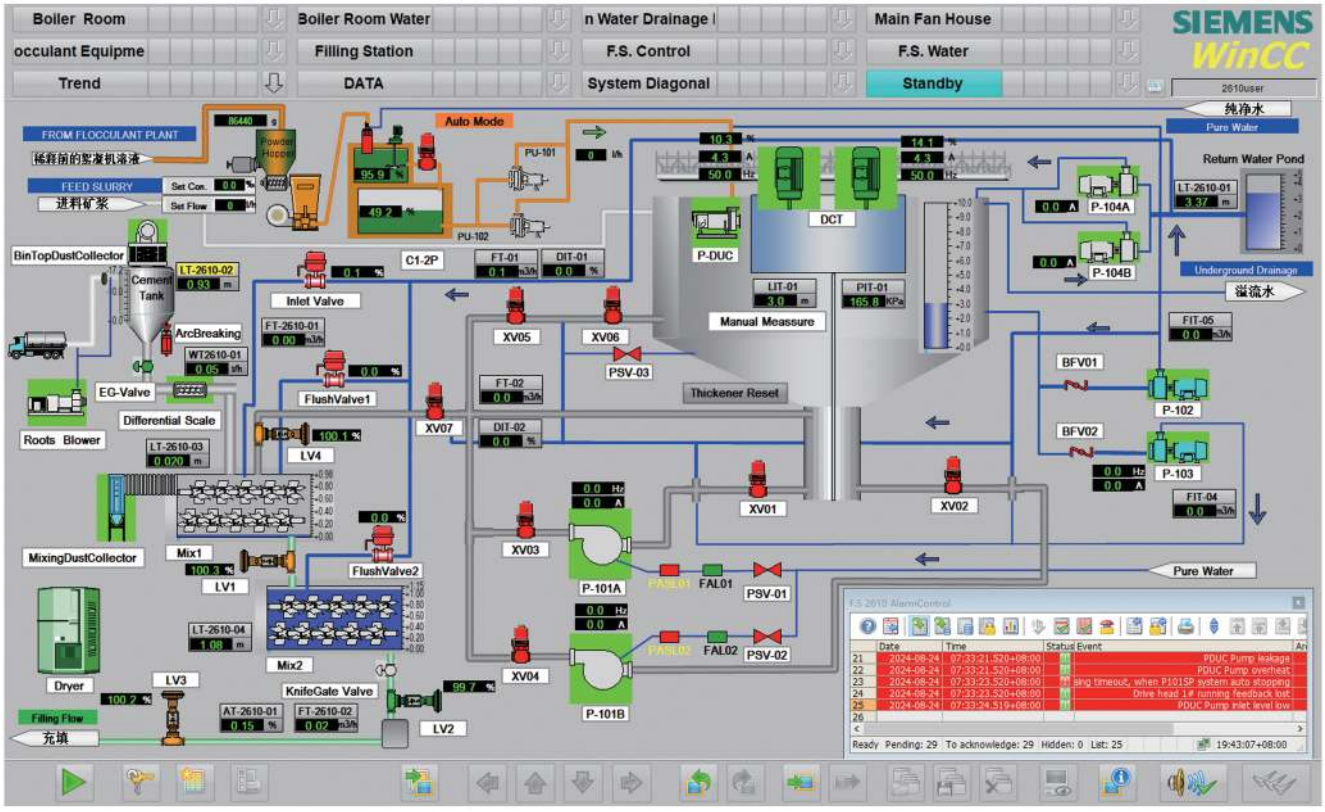

Figure 3 Human–machine interface of the control system

sample, and μ_j and σ_j represent the mean and standard deviation of the j-th feature, respectively. The standardized variable Z_{ij} exhibits a mean of 0 and a standard deviation of 1.

3.2 Sliding window construction and dataset partitioning

Given the short-term dynamic correlation between underflow concentration and recent operating conditions, a sliding time window of length 3 was employed to construct supervised learning samples. Each sample comprised a sequence of four process variables spanning the three most recent time steps, serving to predict the underflow concentration at the subsequent time step. By sliding the window along the time axis, an input tensor of shape (N, 3, 4) and its corresponding target vector were generated, where N denotes the total number of samples. The dataset was partitioned into training and testing sets in chronological order, with the initial 80% designated for training and the final 20% for testing. Within the training set, a further 10% was allocated as a validation subset to facilitate early stopping [15]. This partitioning strategy preserves the temporal integrity of the data by avoiding random shuffling, thereby better reflecting real-world online prediction scenarios.

3.3 LSTM network architecture and training configuration

Although static intelligent models effectively predict material properties, the significant inertia and time-lags of the thickening process (Section 3.1) necessitate a dynamic approach. Unlike standard recurrent neural networks (RNNs) limited by vanishing gradients, the LSTM architecture employs gating mechanisms to effectively retain critical historical information. To capture the nonlinear coupling and temporal dependencies among process variables, a predictive model based on LSTM networks was constructed. The network architecture is depicted in Figure 4, and the associated hyperparameters are listed in Table 2.

To accommodate the interpolated small-sample dataset, a single-layer LSTM architecture with 20 hidden nodes was adopted to balance model capacity and generalization. Incorporating a dropout rate of 0.2, this configuration effectively captured nonlinear couplings while mitigating overfitting. The input sequence length was set to 3 (corresponding to a 15-min time window) to capture rapid dynamic responses of the equipment while minimizing historical noise interference. The ReLU activation function was selected to mitigate vanishing gradients and enhance training stability. Regarding the training strategy, a small batch size (batch size = 8) was employed to introduce stochasticity, thereby facilitating the escape from local optima. An early stopping mechanism (patience = 15)

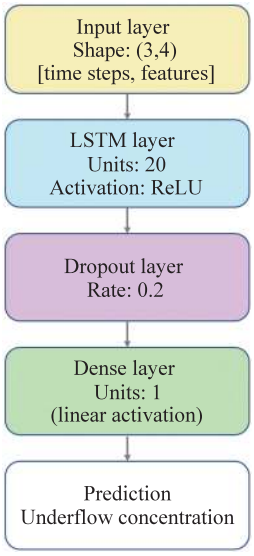

Figure 4 Schematic diagram of the LSTM network architecture

Table 2 Hyperparameters of the LSTM model

Parameter	Setting	Explanation
LSTM units	20	Balances temporal feature extraction and model simplicity
Activation	ReLU	Prevents vanishing gradients
Dropout rate	0.2	Reduces overfitting
Dense units	1	Single regression output
Learning rate	0.01	Empirically stable LR
Optimizer	Adam	Fast and robust convergence
Loss function	MSE	Standard for regression
Batch size	8	Stable for small datasets
Max epochs	150	Ensures sufficient learning
Early stopping patience	15	Stops before overfitting
Radom state	0	Reproduced results

was implemented to terminate training automatically, ensuring optimal generalization performance on the validation set. The model was implemented in Python using the TensorFlow/Keras framework, with the random seed fixed at 0 to ensure result reproducibility. Preliminary comparisons demonstrated the superiority of this recurrent architecture over static linear baselines, which struggled to capture the significant process time-lags.

3.4 Performance evaluation and scenario prediction

Upon training completion, the model performed forward predictions on both the training and test datasets. The predictions were reverted to underflow concentrations (%) through inverse normalization. Model fitting accuracy and generalization performance were evaluated using mean squared error (MSE), mean absolute error (MAE), root mean squared error (RMSE), and coefficient of determination (R^2). While these metrics possess inherent correlations, their simultaneous application offers complementary insights into model reliability. Specifically, R^2 quantifies the model's capacity to capture process variance and trends. Regarding error magnitude, RMSE assigns a higher weight to large deviations, serving as a sensitive indicator for safety-critical anomalies [16], whereas MAE provides a more robust measure of average prediction error. This combined approach ensures a comprehensive evaluation of both routine tracking accuracy and the risk of extreme outliers. The metrics were calculated according to Equations (2)–(5). Notably, MAE and RMSE are expressed in percentage points to facilitate the operational interpretation of error levels.

$$\mathrm{MSE}=\frac{1}{n}\sum_{i=1}^{n}(y_i-\hat{y}_i)^2 \tag{2}$$

$$\mathrm{MAE}=\frac{1}{n}\sum_{i=1}^{n}\left|y_i-\hat{y}_i\right| \tag{3}$$

$$\mathrm{RMSE}=\sqrt{\frac{1}{n}\sum_{i=1}^{n}(y_i-\hat{y}_i)^2} \tag{4}$$

$$R^2=1-\frac{\sum_{i=1}^{n}(y_i-\hat{y}_i)^2}{\sum_{i=1}^{n}(y_i-\overline{y})^2} \tag{5}$$

where n represents the total number of samples; y_i denotes the actual underflow concentration of the i-th sample; $\hat{y}_i$ is the predicted (inverse-normalized) underflow concentration; $\overline{y}$ is the average actual underflow concentration.

Subsequently, scenario simulations for underflow discharge control were conducted using the trained model. Using the final three time steps of historical data as the initial window, three constant underflow discharge scenarios (40, 50, and 60 m^3/h) were established. Underflow concentration was recursively predicted over a 3-h horizon (36 5-min intervals). Simultaneously, a random perturbation of 0.5% was applied to the other three process variables to simulate operational fluctuations. The resulting trajectories under different strategies were analyzed to assess the impact of discharge rates on the evolution of underflow concentration.

4 Results and discussion

4.1 Analysis of model training performance

Figure 5 illustrates the loss curves of the multivariate LSTM model during training. Early stopping was

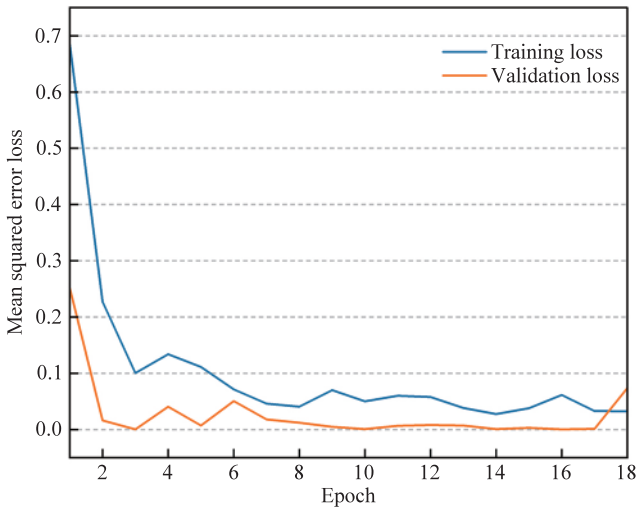

Figure 5 Training and validation loss curves

triggered at the 18th epoch, indicating rapid and stable convergence of the optimization process. This strategy, combined with Dropout regularization, effectively mitigated overfitting to noise.

Figure 6 depicts the scatter plot of predicted versus actual values for the training set. Actual underflow concentrations were primarily distributed within the 74%–80% range, achieving a coefficient of determination (R^2) of 0.92. This indicates that the model effectively captured the mapping between input features and underflow concentration. Notably, fluctuations at the high-concentration end align with the operational characteristics of DCT, where nonlinear amplification and increased stochastic fluctuations occur during high-viscosity regimes. The test set yielded an MAE of 0.42% and an RMSE of 0.48%, both below the typical measurement noise (~0.5%) of industrial radiometric density gauges. This demonstrates that the model's accuracy meets engineering requirements, validating its utility for trend prediction and decision support in DCT operations.

4.2 Prediction of underflow concentration under different discharge scenarios

Multi-step prediction over a 3-h horizon was achieved by employing a recursive sliding window strategy based on the single-step LSTM model, as illustrated in Figure 7. Unlike direct multi-step approaches, this recursive structure facilitates the incorporation of dynamic operational adjustments (e.g., varying discharge rates) at each time step, making it particularly suitable for the control scenario simulations conducted in this study.

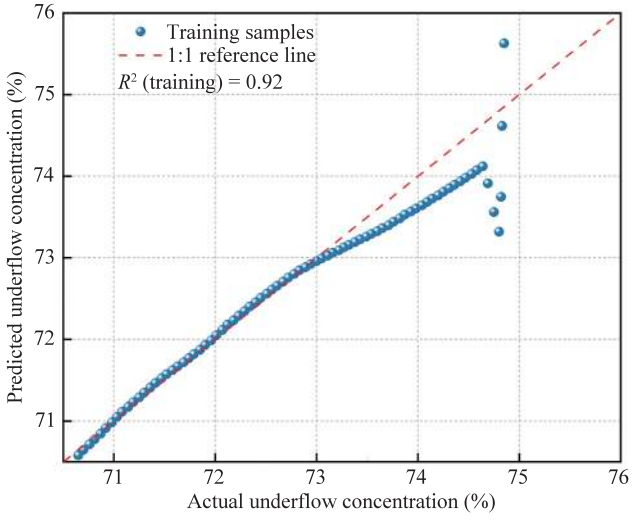

Figure 6 Comparison of predicted versus actual values in the training set

Building upon the strategy, three control scenarios featuring underflow discharge rates of 40, 50, and 60 m^3/h were established. Gaussian perturbations with a relative amplitude of 0.5% were applied to uncontrolled process variables to simulate the minor fluctuations inherent in actual operations. The simulation results (Figure 8) show that while concentrations across all scenarios remained within the 71%–77% range, distinct disparities emerged. At a discharge rate of 40 m^3/h, the underflow concentration remained consistently above 75% throughout the simulation. Frequent local peaks evident in the trajectory suggest a prolonged residence time of the slurry within the thickener at low discharge rates. While this facilitates the formation of high-concentration underflow, the concomitant increase in yield stress and viscosity heightens the risk of rake torque overload and discharge blockages. When the discharge rate was increased to 50 m^3/h, underflow concentrations primarily ranged between 73% and 75%. Compared to the 40 m^3/h scenario, the fluctuation amplitude diminished, indicating that a moderate increase in discharge rate mitigated slurry accumulation within the thickener. Consequently, this broadened the "safe operating window" of the DCT. In the high discharge rate scenario (60 m^3/h), the underflow concentrations further declined to 71%–74%. While advantageous for mitigating rake jamming, this scenario presents challenges for the paste filling process. Excessively low underflow solids content complicates paste consistency control, potentially compromising the mechanical strength of the backfill.

Consequently, neither maximizing nor minimizing discharge rates constitutes an optimal strategy; a balance must be struck between operational safety and backfill quality. The LSTM-based intelligent prediction model proposed herein facilitates discharge rate control by simulating future underflow concentration trajectories. Adopting a "predicting–evaluating–regulating" paradigm, the model shifts the control

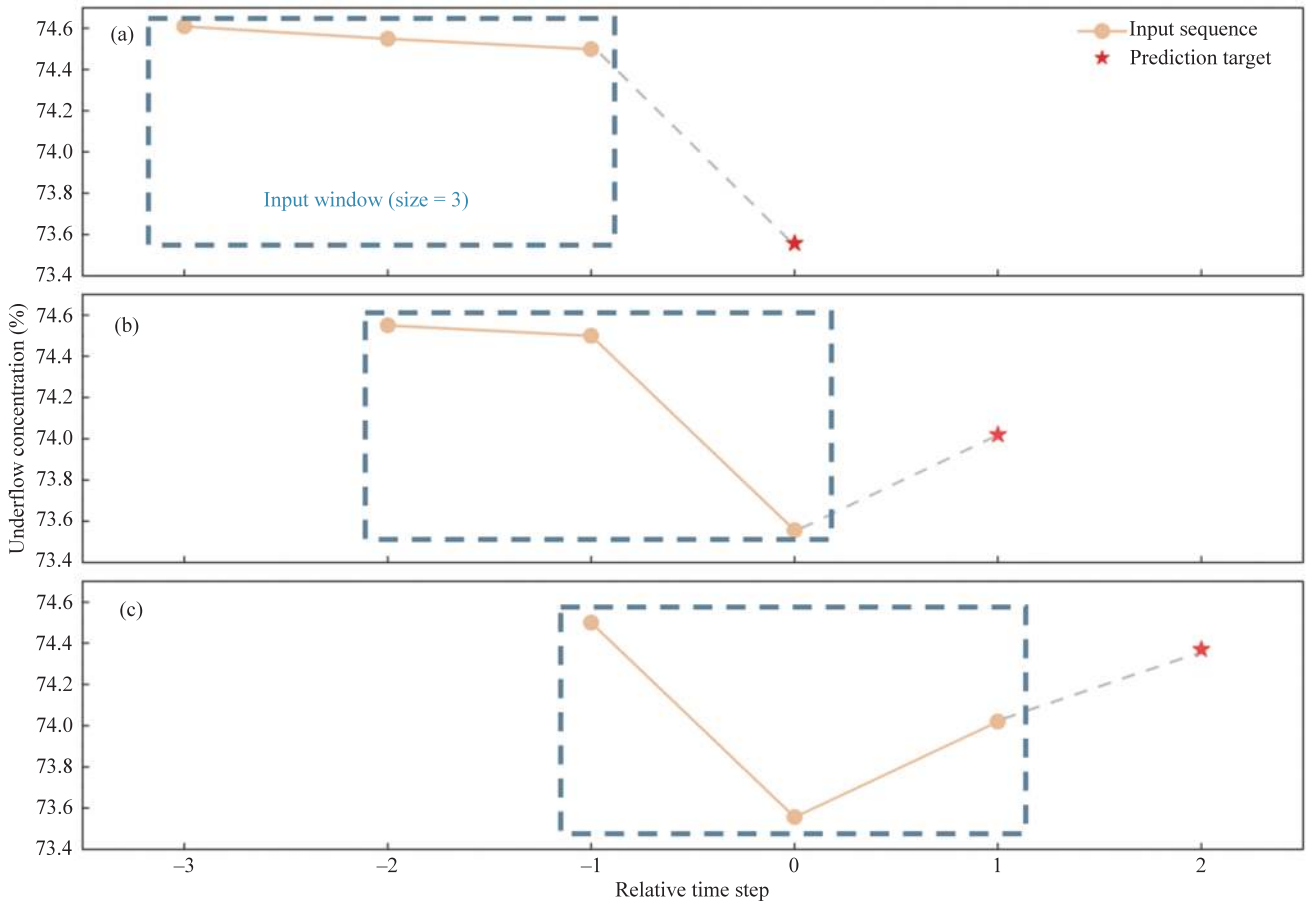

Figure 7 Schematic illustration of the sliding-window mechanism used to construct input–output pairs for the LSTM model. (a) Initial input window consisting of historical observations for predicting T+1. (b) Sliding the window to include the prediction at T+1 for predicting T+2. (c) Further sliding the window to include the prediction at T+2 for predicting T+3

strategy from reactive feedback to proactive prevention. This provides a reliable technical pathway for the intelligent, precision management of DCT.

4.3 Field application results of high-density whole-tailings thickening and paste filling

The LSTM-based prediction model facilitates the coordinated operation of the paste filling process—from thickening and dewatering to paste preparation and underground placement. Industrial trials demonstrated that the DCT achieved dynamic equilibrium under deep bed compaction conditions, with the bed depth reaching a maximum of 5.5 m. Under feed slurry flow rates of 70–90 m^3/h and concentrations of 45%–50%, the system maintained stable operation for over 7 consecutive hours by regulating underflow discharge. Consequently, underflow concentration was sustained between 70% and 82% (Figure 9). This effectively mitigated the impact of feed fluctuations on underflow quality, ensuring the continuous output of high-concentration slurry.

Notably, the underflow concentration decreased from 82% to 70% after 7 h, while still meeting the requirement for preparing 74%–76% paste. This decline was primarily attributed to an imbalance between feed and discharge mass flow. The mass balance between dry feed and dry discharge can be calculated using Equation (6). The definitions of the symbols used in Equation (6) are listed in Table 3.

$$\Delta M = Q_{out} \cdot \rho_{out} \cdot C_{out} - Q_{in} \cdot \rho_{in} \cdot C_{in} \quad (6)$$

The observed decrease in underflow concentration (from 82% to 70%) suggests that $\Delta M > 0$, implying that the dry discharge mass rate continuously exceeded the dry feed mass rate. Consequently, the slurry bed level descended, leading to a steady decrease in underflow

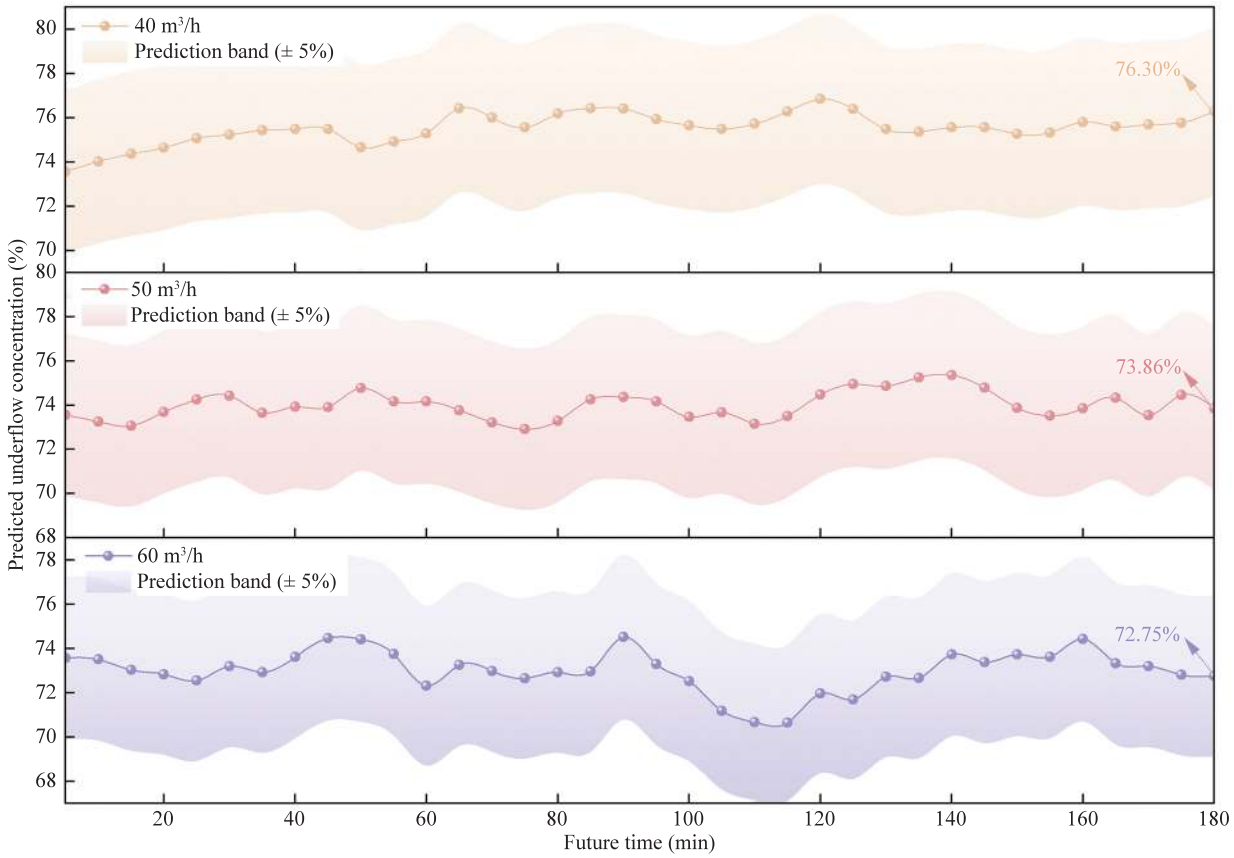

Figure 8 Predicted underflow concentration over the next 3 h under different underflow rates

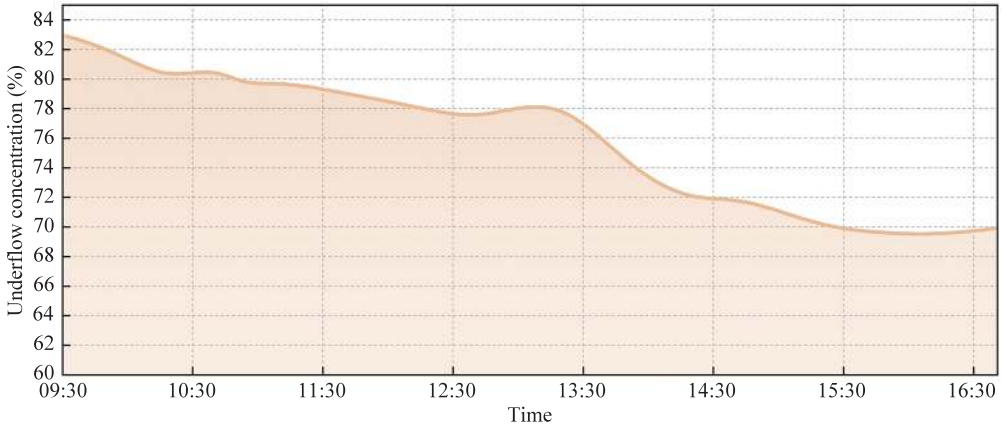

Figure 9 Time series of underflow concentration

concentration. The bed depth and discharge conditions achieved during commissioning ensured continuous and stable filling with high-density tailings for 7 h, satisfying the production capacity requirements of the mining stopes.

The high solids content of the supplied underflow ensured the homogeneity and stability of paste preparation. For underflow concentrations exceeding the optimal range (e.g., reaching the maximum of 82%), dilution water was used to adjust the final mixture. The paste solids content was stably controlled between 74% and 76%, with a yield stress of approximately 55–70 Pa, meeting the rheological requirements for pipeline transport. The macroscopic appearance of the paste is depicted in Figure 10. Figure 11 indicates that an underflow concentration

Table 3 Nomenclature of mass balance variables

Symbol	Description	Unit
ΔM	Dry mass differential rate	t/h
Q_{out}	Discharge volumetric flow rate	m^3/h
ρ_{out}	Discharge slurry density	t/m^3
C_{out}	Discharge mass concentration	%
Q_{in}	Feed volumetric flow rate	m^3/h
ρ_{in}	Feed slurry density	t/m^3
C_{in}	Feed mass concentration	%

between 70% and 76% suffices to meet the targets for paste preparation. Furthermore, paste solids content exhibits a strong positive correlation with underflow concentration, highlighting the critical role of upstream thickening control in supporting downstream preparation.

The prepared paste was transported via pipelines to the underground stopes, filling the upward horizontal cut-and-fill mining faces. The bottom 2 m layer employed low-strength backfill with a 1:10 binder-to-tailings ratio, achieving initial set within 10 h and meeting the bearing capacity requirements for personnel access. The top 0.5 m capping layer utilized high-strength paste with a 1:4 binder-to-tailings ratio, reaching a strength of 1.5 MPa after 1 day of curing and exceeding 3 MPa within 3 days. The on-site backfill results are presented in Figure 12. The discharge from the pipe outlet was uniform, and after curing, the backfill body exhibited tight bonding with the surrounding rock.

5 Conclusions

Based on industrial commissioning and data analysis of the high-density whole-tailings thickening and paste backfill process at the Ovoo Zinc Mine, an LSTM-based underflow concentration prediction model was developed and applied to a proactive control strategy for underflow discharge rates. The key conclusions are summarized as follows:

(1) A high-precision time-series prediction model for underflow concentration was constructed. By integrating strategies such as *Z*-score normalization, Dropout regularization, and early stopping, the model's generalization capability and training stability were effectively enhanced. The model demonstrated robust fitting performance on the training set (R^2 = 0.92) and achieved an MAE of 0.42% and RMSE

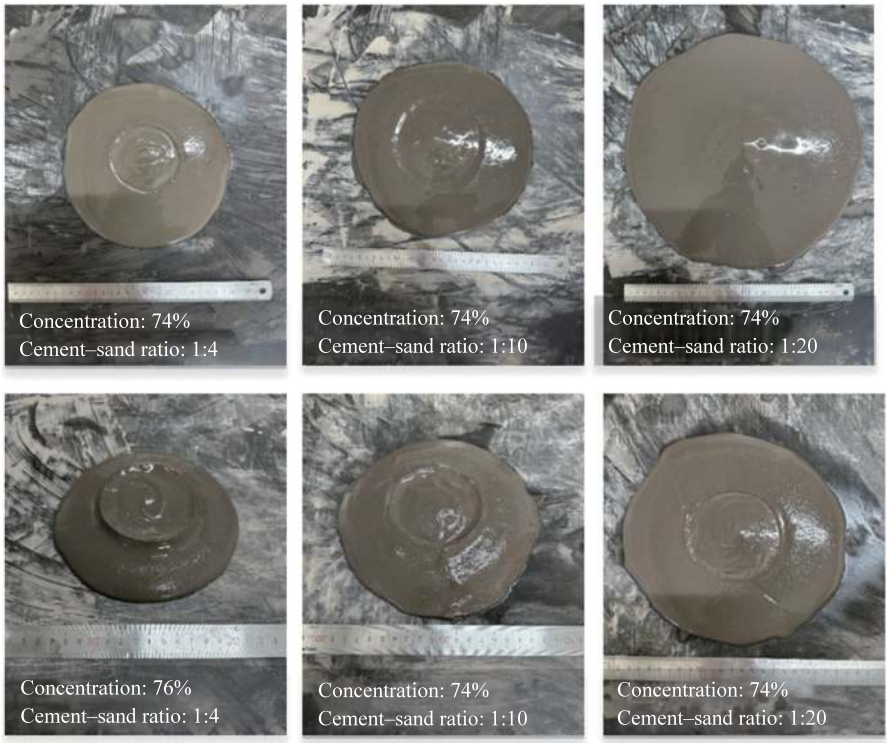

Figure 10 Macroscopic appearance of paste under different solids contents and binder-to-tailings ratios

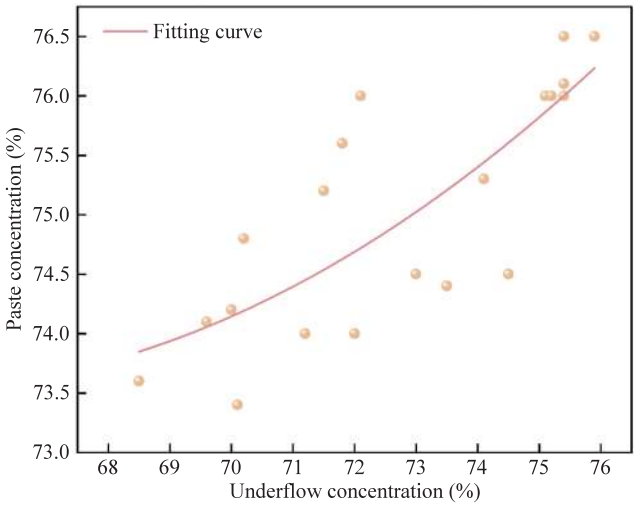

Figure 11 Relationship between paste solids content and underflow concentration

Figure 12 Performance of underground backfill. (a) Paste discharge at the outlet. (b) Cured state of the backfill body

of 0.48% on the test set, thereby meeting the requirements for process trend prediction in paste backfill.

(2) A proactive feedforward control strategy of "predicting–evaluating–regulating" was proposed. Leveraging the scenario simulation capabilities of the LSTM model, the study quantitatively revealed the nonlinear relationship between underflow discharge rate and underflow concentration. This approach effectively mitigates risks such as rake torque overload or compromised backfill strength associated with extreme discharge rates. By shifting the paradigm from "lagging feedback" to "proactive prevention," the system's robustness against disturbances and operational stability were enhanced.

(3) Industrial test results indicate that, under the guidance of the intelligent model, the DCT maintained dynamic equilibrium under deep-bed compaction conditions with a slurry bed depth of approximately 5.5 m, even when subjected to fluctuating feed slurry flow rates. The underflow concentration remained stable between 70% and 80% for seven consecutive hours. The paste preparation concentration remained consistently stable at 74%–76%, exhibiting favorable rheological properties. The underground backfill exhibited strong early-age mechanical performance, reaching 1.5 MPa after one day of curing and exceeding 3 MPa after three days.

Acknowledgements

The authors thanks for the funding support from the National Key Research and Development Program of China (No. 2025YFE0212200), the China-Zambia Belt and Road Joint Laboratory on Green and Safe Development of Mineral Resources, and Fundamental Research Funds for the Central Universities (No. FRF-TP-24-047A).

Declarations

The authors declare that they have no conflict of interests.

References

[1] A. Wu, Y. Wang, Z. Ruan, B. Xiao, J. Wang, and L. Wang, "Key theory and technology of cemented paste backfill for green mining of metal mines," *Green and Smart Mining Engineering*, Vol. 1, pp. 27–39, 2024.

[2] S. Yin, Y. Shao, A. Wu, H. Wang, X. Liu, and Y. Wang, "A systematic review of paste technology in metal mines for cleaner production in China," *Journal of Cleaner Production*, Vol. 247, p. 119590, 2020.

[3] A. Tariq, and E. K. Yanful, "A review of binders used in cemented paste tailings for underground and surface disposal practices," *Journal of Environmental Management*, Vol. 131, pp. 138–149, 2013.

[4] D. Balthazar, L. Fleming, and E. Vlot, "Case study: Brucejack paste backfill pumping system," Proceedings of the 25th International Conference on Paste, Thickened and Filtered Tailings (Paste 2023), Banff, Canada, pp. 40–46, 2023.

[5] S. Barrera, and J. Engels, "High-density thickening for large production rates: main challenges," Proceedings of the 21st International Seminar on Paste and Thickened Tailings (Paste 2018), Perth, Australia, pp. 35–42, 2018.

[6] C. K. Tan, J. Bao, and G. Bickert, "A study on model predictive control in paste thickeners with rake torque constraint," *Minerals Engineering*, Vol. 105, pp. 52–62, 2017.

[7] C. G. Olmedo, A. R. Gomez, D. G. Limon Galindo, and J.

A. B. Muñoz, "Revisión de los equipos de decantación para estériles de mina: del espesador convencional al de cono profundo para la producción de pasta," *DYNA*, Vol. 90, pp. 359–365, 2015. (in Spanish)

[8] J. Ruuska, R.-P. Nikula, E. Ruhanen, J. Kauppi, S. Kauvosaari, and M. Kosonen, "Data analysis of a paste thickener," *Open Engineering*, Vol. 10, pp. 362–367, 2020.

[9] J. I. Langlois, and A. Cipriano, "Dynamic modeling and simulation of tailing thickener units for the development of control strategies," *Minerals Engineering*, Vol. 131, pp. 131–139, 2019.

[10] M. Kosonen, S. Kauvosaari, S. Gao, and B. Henriksson, "Performance optimization of paste thickening," Proceedings of the 20th International Seminar on Paste and Thickened Tailings (Paste 2017), Beijing, China, pp. 13–22, 2017.

[11] R. Oulhiq, K. Benjelloun, Y. Kali, M. Saad, and H. Griguer, "Constrained model predictive control of an industrial high-rate thickener," *Journal of Process Control*, Vol. 133, p. 103147, 2024.

[12] A. Graves, "Long short-term memory." in *Supervised Sequence Labelling with Recurrent Neural Networks*. Berlin: Springer, pp. 37–45, 2012.

[13] D. Quesada, G. Valverde, P. Larrañaga, and C. Bielza, "Long-term forecasting of multivariate time series in industrial furnaces with dynamic Gaussian Bayesian networks," *Engineering Applications of Artificial Intelligence*, Vol. 103, p. 104301, 2021.

[14] Y. Lei, and H. R. Karimi, DualLSTM: A novel key-quality prediction for a hierarchical cone thickener. *Control Engineering Practice*, Vol. 137, p. 105566, 2023.

[15] L. Prechelt, "Early stopping-but when?" in *Neural Networks: Tricks of the Trade*, G. B. Orr, and K.-R. Müller (Eds.), Springer, Berlin, pp. 55–69, 1998.

[16] T. Chai, and R. R. Draxler, "Root mean square error (RMSE) or mean absolute error (MAE)?—Arguments against avoiding RMSE in the literature," *Geoscientific Model Development*, Vol. 7, no. 3, pp. 1247–1250, 2014.